Electronic Supplementary Information For

Fluorescent aptasensing of chlorpyrifos based on assembly of cationic conjugated polymer-aggregated gold nanoparticles and luminescent metal-organic frameworks

Qingju Liu[a,b], Hui Wang[a,b], Ping Han*[a,b], Xiaoyuan Feng[*a,b]

a Beijing Research Center for Agriculture Standards and Testing, Beijing 100097, China;

b Risk Assessment Lab for Agro-products (Beijing), Ministry of Agriculture, Beijing 100097, China

*Corresponding author:

Tel/Fax: (010) 51503564

E-mail: hanp@brcast.org.cn, fengxiaoyuan2014@126.com
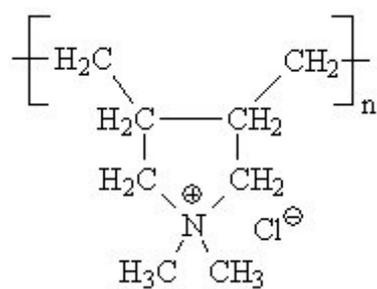
Fig. S1 The structure of poly dimethyl dialyl ammonium chloride (PDDA)
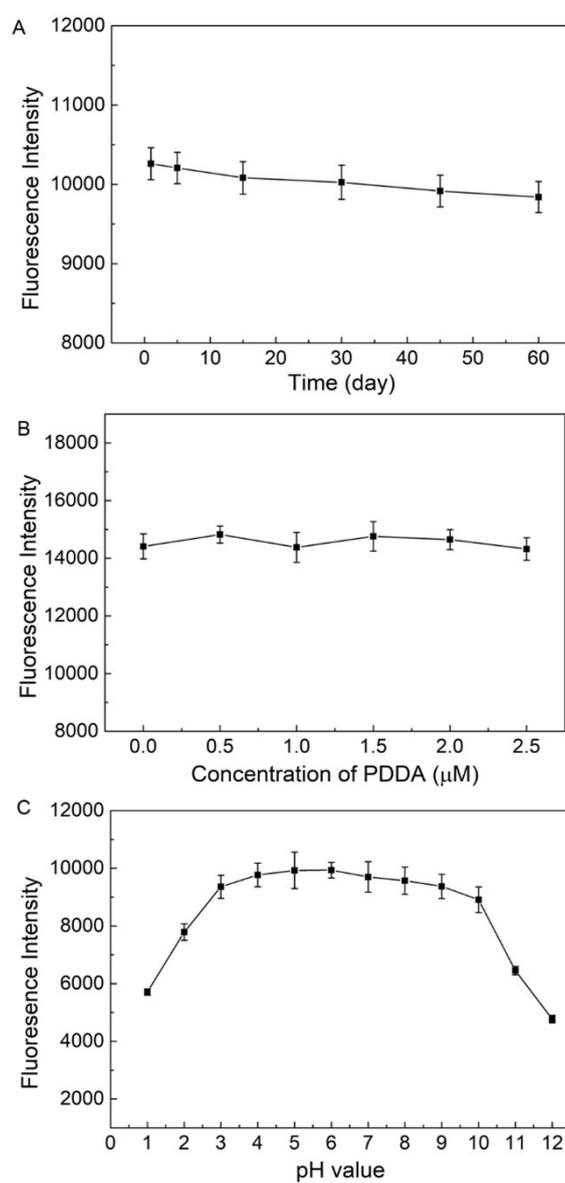
Fig. S2 The effect of time (A), concentration of PDDA (B) and pH value (C) on the fluorescence

intensity of Tb-MOF.
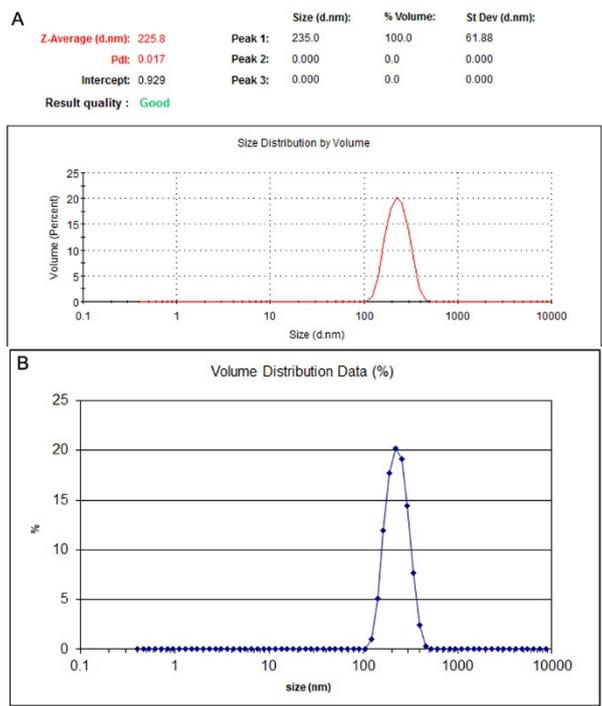
Fig. S3 The dynamic light scattering analysis (A) and volume distribution data of Tb-MOFs (B).
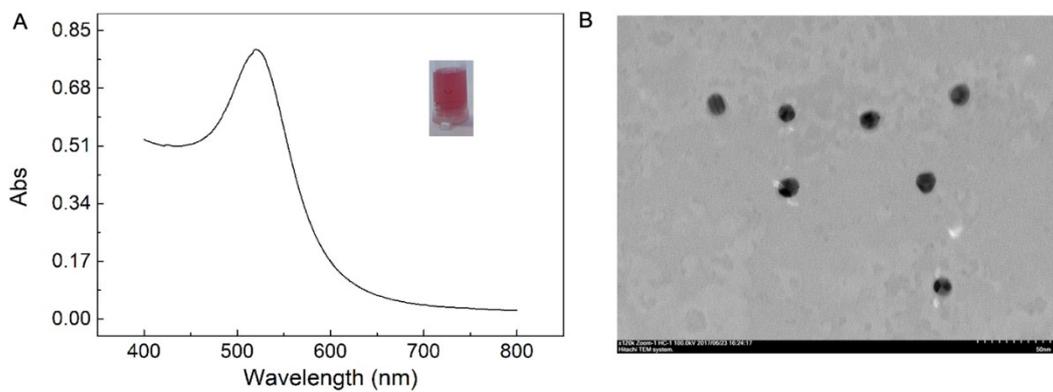
Fig. S4 Characterization of AuNPs by UV (A) and TEM (B).
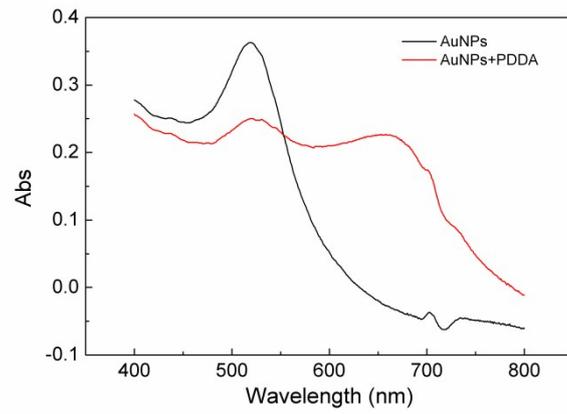
Fig.S5 The UV-vis of AuNPs in the absence (A) and presence (B) of PDDA.
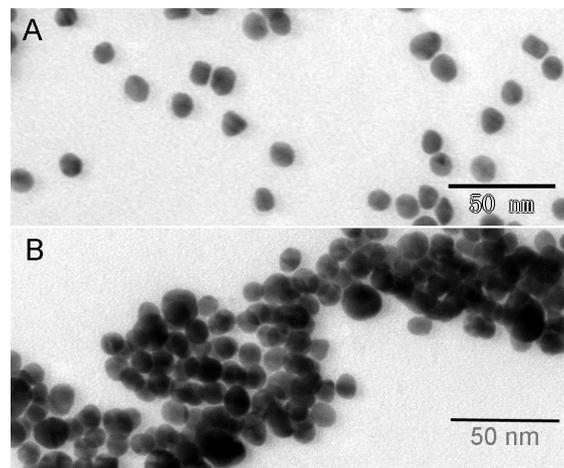
Fig.S6 The TEM image of AuNPs in the absence (A) and presence (B) of PDDA.
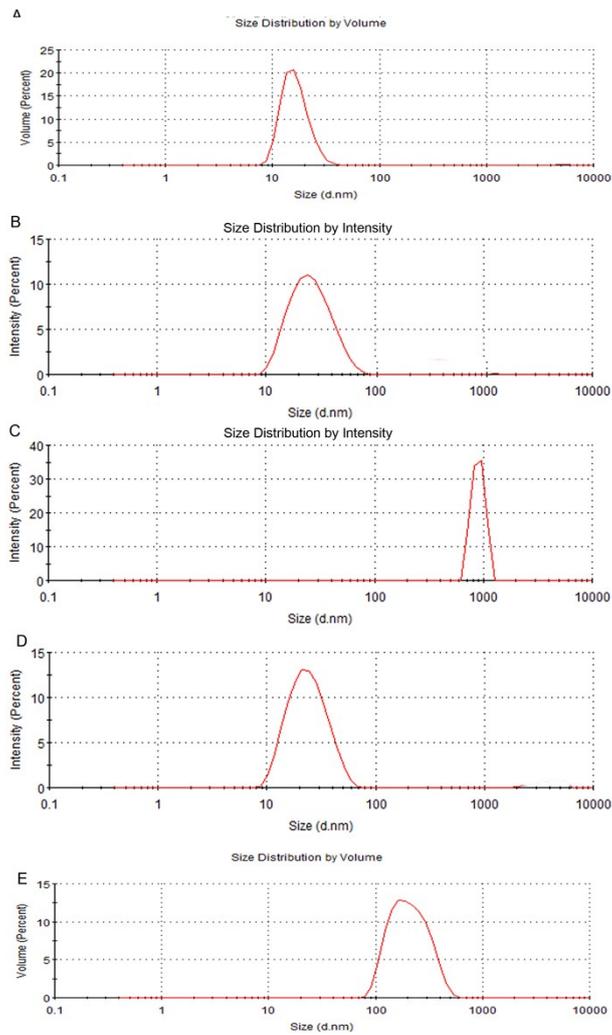
Fig. S7 DLS measurements for AuNPs (A), aptamer-AuNPs (B), PDDA-AuNPs (C), aptamer-AuNPs-

PDDA (D), PDDA-AuNPs-aptamer-CPF-AuNPs (E).
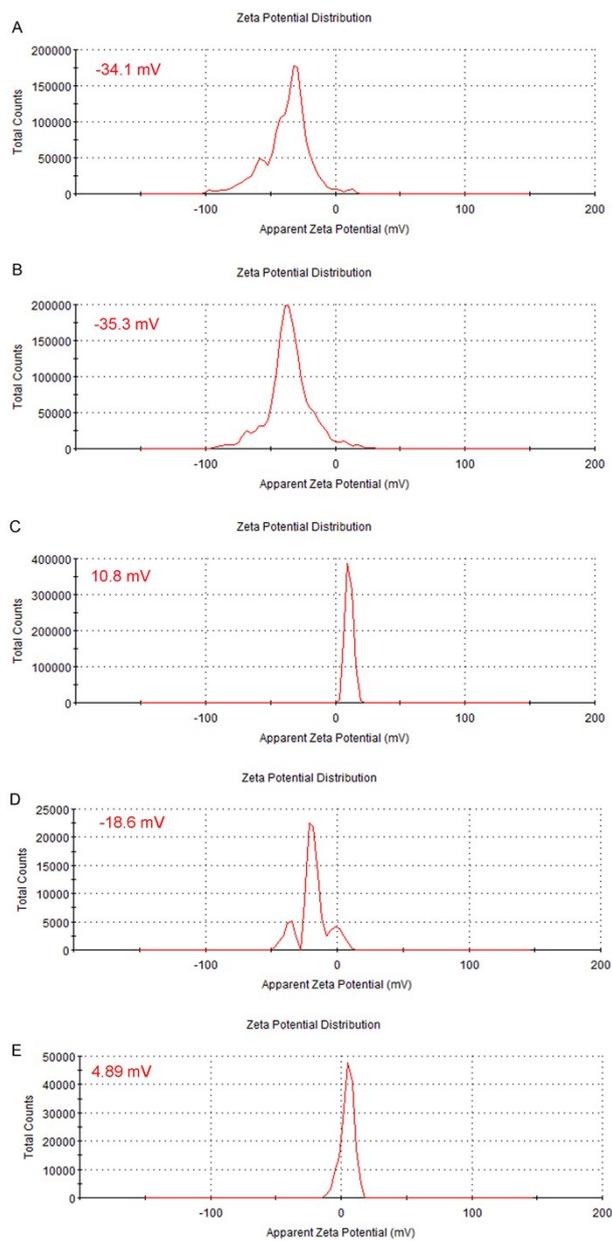
Fig. S8 Zeta potential of AuNPs (A), AuNPs+aptamer (B), AuNPs+PDDA, (C),

AuNPs+aptamer+PDDA(D), AuNPs+aptamer+PDDA+CPF (E).

Table S1 Hydrodynamic diameter and zeta potential of nanoparticles measurement using DLS and zeta potential

Name	DLS d_h (nm)	Zeta potential (mV)
Citrate capped AuNPs	19.8 ± 1.0	-39.9 ± 4.2
AuNPs+aptamer	27.4 ± 1.4	-35.8 ± 1.7
AuNPs+PDDA	1079.9 ± 72.0	10.8 ± 0.6
AuNPs+aptamer+PDDA	20.90 ± 1.1	18.6 ± 0.3
AuNPs+aptamer+PDDA+CPF	197.0 ± 7.7	4.89+0.2
Tb-MOF	222.7 ±6.5	34.4 ± 0.4
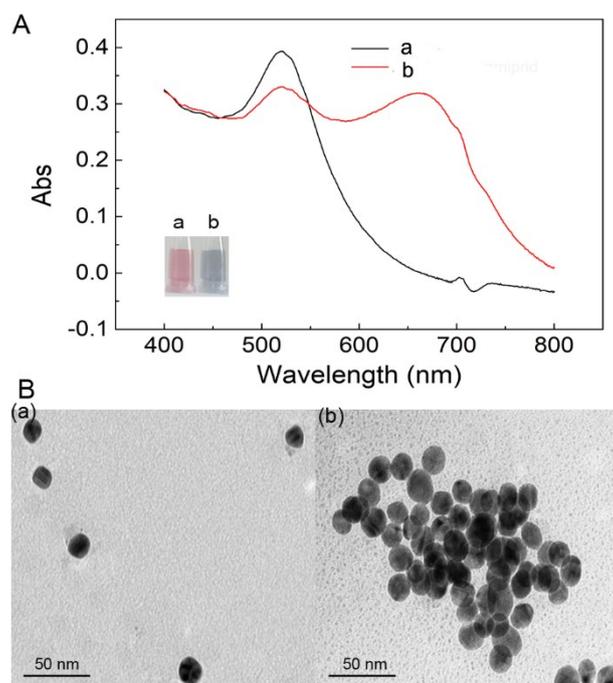
Fig. S9 UV-vis (A) and TEM analysis (B) of AuNPs solution containing aptamer and PDDA (a), AuNPs solution containing aptamer, PDDA and CPF (b).
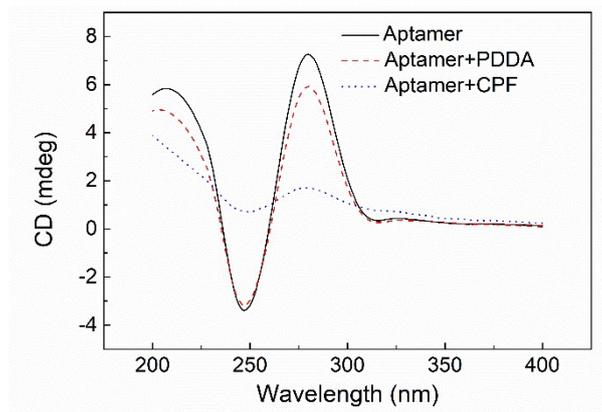
Fig.S10 CD spectra of CPF aptamer solutions treated with PDDA and CPF. Experimental conditions:

10 μM aptamer, 20 μM PDDA and 50 nM CPF.
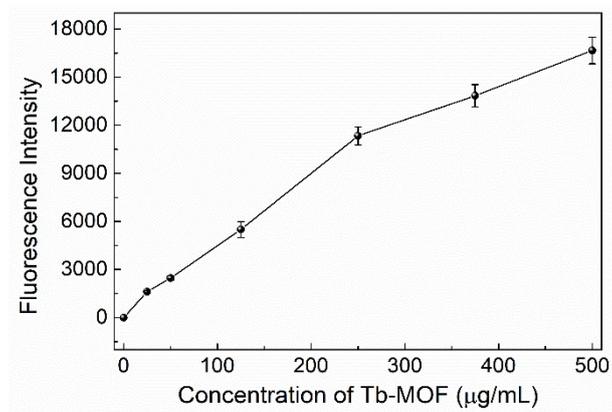
Fig.S11 Optimization of concentration of Tb-MOF
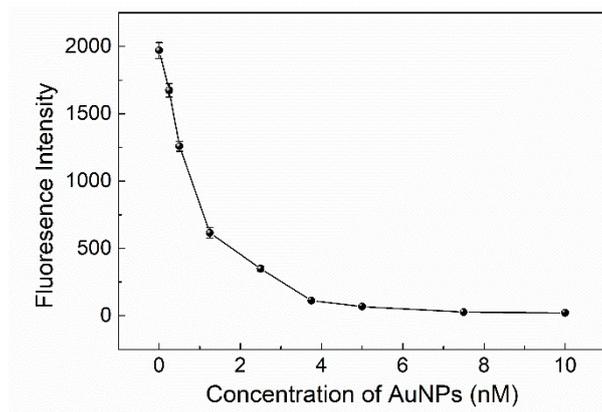
Fig. S12 Optimization of concentration of AuNPs
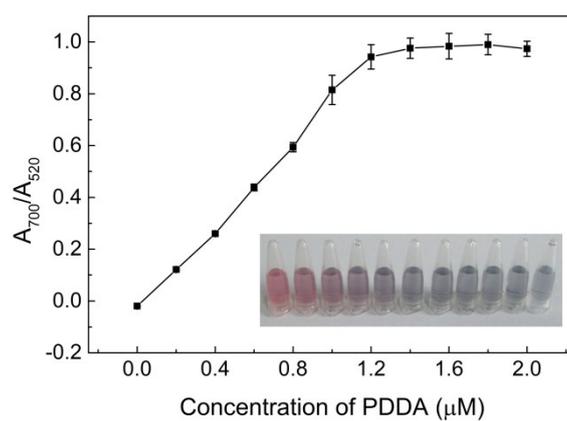
Fig.S13 The calibration curve to optimize PDDA concentration for CPF detection treated with varying concentration of PDDA. The inset figure represents the visual color changes of the AuNPs solutions at each concentration. Error bars represent the standard deviations of three repeated measurements.
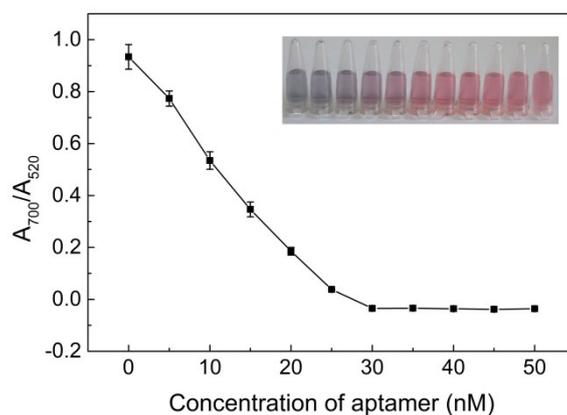
Fig.S14 The calibration curve to optimize aptamer concentration for CPF detection treated with varying concentration of aptamer against PDDA. The concentration of PDDA is 1.4 µM. The inset figure represents the visual color changes of the AuNPs solutions at each concentration. Error bars represent the standard deviations of three repeated measurements.
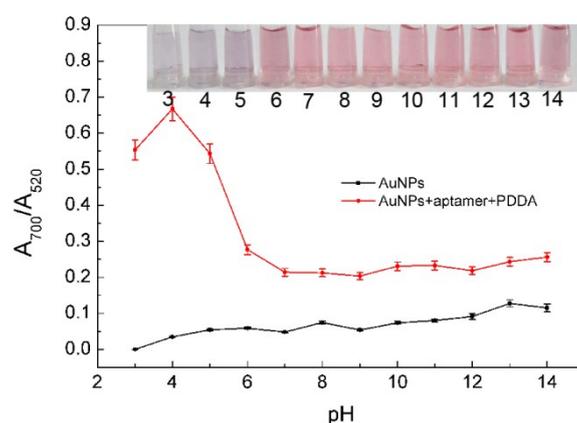
Fig.S15 The calibration curve to optimize pH value for CPF detection treated with aptamer against PDDA. The concentration of PDDA and aptamer are 1.4 µM and 30 nM, respectively.The inset figure represents the visual color changes of the AuNPs solutions at each pH value.
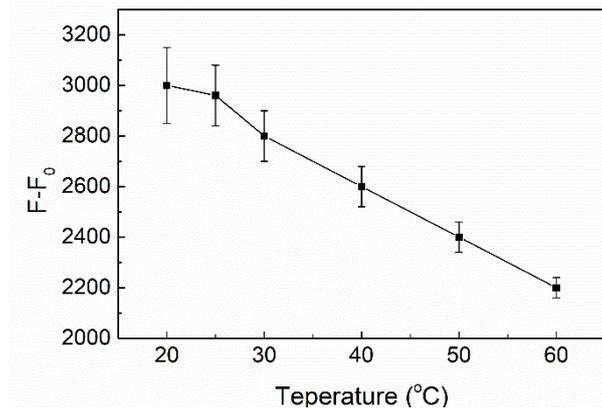
Fig. S16 Optimization of temperature.
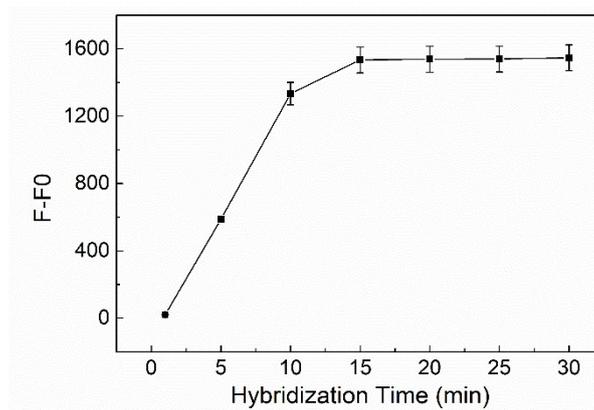
Fig. S17 The calibration curve to optimize hybridizationtime for CPF detection treated with aptamer against PDDA. The concentration of CPF, PDDA and aptamer are 50 nM, 1.4 μM and 30 nM, respectively. Error bars represent the standard deviations of three repeated measurements.
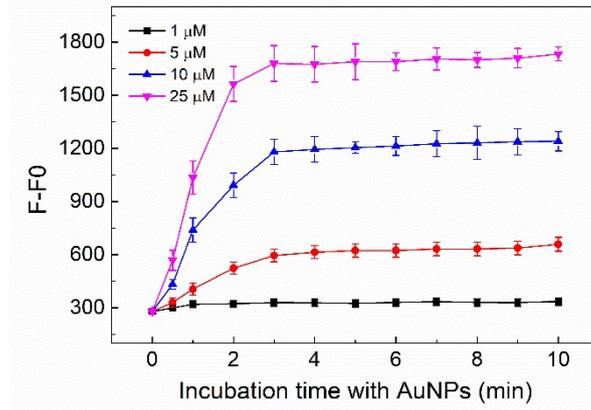
Fig. S18 Kinetics of the F-F$_0$ in the sensing system treated with different concentrations of CPF. The concentration of PDDA and aptamer are 1.4 µM and 6 nM, respectively. Error bars represent the standard deviations of three repeated measurements.
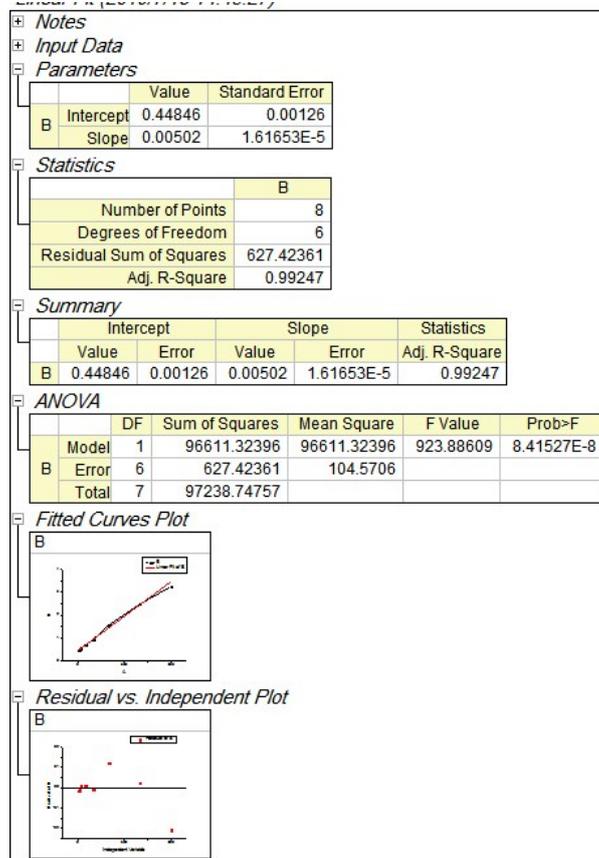
Fig.S19 The linear fit of curve of F-F$_0$ value vs CPF concentration at low concentration.
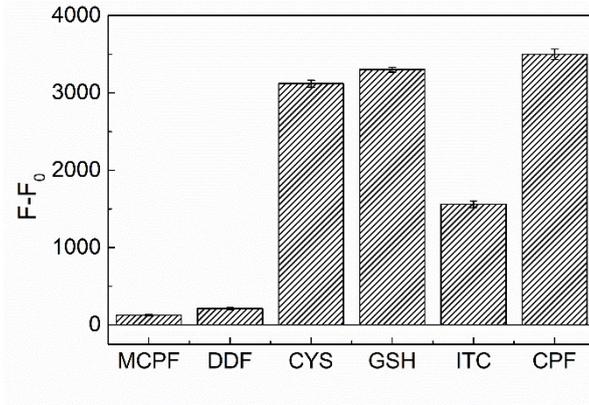
Fig. S20 The selectivity of the method with co-existences in the vegetables.